A satellite orbit drift in binary near-Earth asteroids (66391) 1999 KW4 and (88710) 2001 SL9 — Indication of the BYORP effect

P. Scheirich [a,*], P. Pravec [a], P. Kušnirák [a], K. Hornoch [a], J. McMahon [b], D. J. Scheeres [b], D. P. Pray [c], H. Kučáková [a], A. Galád [d], J. Vraštil [a], Yu. N. Krugly [e], N. Moskovitz [f], R. S. McMillan [g], J. A. Larsen [g,h], M. J. Brucker [g], A. F. Tubbiolo [g], W. R. Cooney [i], J. Gross [i], D. Terrell [i,j], O. Burkhonov [k], P. Fatka [a], R. Durkee [ℓ], E. Schunova [m], R. Ya. Inasaridze [n,o], N. M. Gaftonyuk [p]

[a] *Astronomical Institute, Academy of Sciences of the Czech Republic, Fričova 1, CZ-25165 Ondřejov, Czech Republic*

[b] *Department of Aerospace Engineering Sciences, The University of Colorado at Boulder, Boulder, CO, USA*

[c] *Sugarloaf Mountain Observatory, South Deerfield, MA, USA*

[d] *Modra Observatory, Department of Astronomy, Physics of the Earth, and Meteorology, FMPI UK, Bratislava SK-84248, Slovakia*

[e] *Institute of Astronomy of Kharkiv National University, Sumska Str. 35, Kharkiv 61022, Ukraine*

[f] *Lowell Observatory, 1400 W Mars Hill Road, Flagstaff, AZ 86001, USA*

[g] *Lunar and Planetary Laboratory, University of Arizona, 1629 East University Boulevard, Tucson, AZ 85721, USA*

[h] *U.S. Naval Academy, Annapolis, MD, USA*

[i] *Sonoita Research Observatory, 77 Paint Trail, Sonoita, AZ 85637, USA*

[j] *Deptartment of Space Studies, Southwest Research Institute, Boulder, CO 80302, USA*

[k] *Ulugh Beg Astronomical Institute, Astronomicheskaya Street 33, 100052 Tashkent, Uzbekistan*

[ℓ] *Shed of Science South Observatory, Pontotoc, TX, USA*

[m] *University of Hawaii, Honolulu, HI, USA*

[n] *Kharadze Abastumani Astrophysical Observatory, Ilya State University, K. Cholokashvili Avenue 3/5, Tbilisi 0162, Georgia*

[o] *Samtskhe-Javakheti State University, Rustaveli Street 113, Akhaltsikhe 0080, Georgia*

Preprint submitted to Elsevier Preprint *21 August 2019*

[p] *Crimean Astrophysical Observatory of Russian Academy of Sciences, 298409 Nauchny, Ukraine*

Proposed running head: XXXX

Editorial correspondence to:
Peter Scheirich, Ph.D.
Astronomical Institute AS CR
Fričova 1
Ondřejov
CZ-25165
Czech Republic
Phone: 00420-323-620115
Fax: 00420-323-620263
E-mail address: petr.scheirich@gmail.com

Abstract

XXXX

Key words: Asteroids, dynamics; Near-Earth objects; Photometry

* Corresponding author. Fax: +420 323 620263.

Email address: petr.scheirich@gmail.com (P. Scheirich).

1 Introduction

Binary near-Earth asteroids may exhibit interesting mutual dynamics driven by re-radiation of light off an irregularly shaped components (see Section 5), but there is only one study constraining its limits based on a direct measurements so far (Scheirich et al., 2015). In this paper, we introduce another comprehensive analysis of two well-observed binary near-Earth asteroids (NEAs).

The NEA (66391) 1999 KW4 (hereafter referred to as 1999 KW4) was discovered by Lincoln Near-Earth Asteroid Research in Socorro, New Mexico, on 1999 May 20. Its binary nature was revealed by Benner et al. (2001). The asteroid was observed thoroughly during six apparitions from 2000 to 2019.

The NEA (88710) 2001 SL9 (hereafter referred to as 2001 SL9) was discovered by Near-Earth Asteroid Tracking at Palomar on 2001 September 18. Its binary nature was revealed by Pravec et al. (2001). The asteroid was observed during five apparitions from 2001 to 2015.

Among the binary NEAs known so far, our photometric dataset of these two sytems are one of the longest coverages obtained, providing a unique opportunity to study an evolution of the mutual orbits of components of small binary asteroids.

The structure of this paper is as follows. In Section 2, we present a model of the mutual orbit of the components of 1999 KW4 and 2001 SL9 constructed from our complete photometric datasets. Then in Sections 3 and 4, we summarize our results with already known parameters of the two binaries. In Section 5, we then discuss implications of the observed characteristics, especially on the BYORP theory, from the derived drifts of the mutual orbits.

2 Mutual orbit models of 1999 KW4 and and 2001 SL9

2.1 Observational data

Table 1
Observations of (66391) 1999 KW4

Time span	No. of nights	Telescope	References
2000-05-24.9 to 2000-06-29.0	XXXX	XXXX	XXXX
2001-05-25.0 to 2001-06-20.9	XXXX	XXXX	XXXX
2016-06-07.9 to 2016-06-22.3	6	0.65-m Ondřejov	This work
	6	0.5-m Sugarloaf Mountain	This work
2017-06-01.8 to 2017-06-27.0	8	0.65-m Ondřejov	This work
	6	0.5-m Sugarloaf Mountain	This work
2018-06-05.9 to 2018-06-18.9	9	0.65-m Ondřejov	This work
2019-05-31.1 to 2019-06-09.2	6	1.8-m Spacewatch	This work
	6	0.65-m Ondřejov	This work
	5	0.5-m Sonoita	This work
	3	0.5-m Sugarloaf Mountain	This work
	3	0.5-m Shed of Science South	This work

References: XXXX

Table 2
Observations of (88710) 2001 SL9

Time span	No. of nights	Telescope	References
2001-10-10.9 to 2001-10-21.3	7	0.65-m Ondřejov	P06
	2	0.5-m Palmer Divide	P06
2012-09-11.9 to 2012-11-15.4	4	1.54-m La Silla	This work
	4	1.5-m Maidanak	This work
2013-10-12.0 to 2013-12-05.1	7	1.54-m La Silla	This work
	2	0.7-m Abastumani	This work
	1	1.0-m Simeiz	This work
2014-10-18.0 to 2014-10-26.1	4	1.54-m La Silla	This work
2015-07-09.2 to 2015-08-17.3	6	XXXX-m Lowell	This work
	3	2.2-m U. Hawaii	This work

References: XXXX

Table 3
Observational stations

Telescope	Observatory	References for observational and reduction procedures
XXX	XXX	XXX

References: XXXX

The data used in our analysis, obtained during six and five apparitions for 1999 KW4 and 2001 SL9, respectively, are summarized in Tables 1 and 2. The references and descriptions of observational procedures of the individual observatories are summarized in Table 3.

The data were reduced using the standard technique described in Pravec et al. (2006). By fitting a two-period Fourier series to data points outside mutual (occultation or eclipse) events, the rotational lightcurves of the primary (short-period) and the secondary (long-period), which are additive in intensities, were separated. The long-period component containing the mutual events and the secondary rotation lightcurve is then used for subsequent numerical modeling (Sect. 2.2).

2.2 Numerical model

We constructed models of the two binary asteroids using the technique of Scheirich and Pravec (2009) that was further developed in Scheirich et al. (2015). In the following, we outline the basic points of the method, but we refer the reader to the 2009 and 2015 papers for details of the technique.

The shapes of the binary asteroid components were represented with ellipsoids, orbiting each other on a Keplerian orbit with apsidal precession and allowing for a quadratic drift in mean anomaly. The primary was modeled as an oblate spheroid, with its spin axis assumed to be normal to the mutual orbital plane of the components (i.e., assuming zero inclination of the mutual orbit). The shape of the secondary was modeled as a prolate spheroid in synchronous rotation, with its long axis aligned with the centers of the two bodies (i.e., assuming zero libration). The shapes were approximated with 1016 and 252 triangular facets for the primary and the secondary, respectively. The components were assumed to have the same albedo. The brightness of the system as seen by the observer was computed as a sum of contributions from all visible facets using a ray-tracing code that checks which facets are occulted by or are in shadow from the other body. A combination of Lommel-Seeliger and Lambert scattering laws was used (see, e.g., Kaasalainen et al., 2002).

The quadratic drift in mean anomaly, ΔM_d, was fitted as an independent parameter. It is the coefficient in the second term of the expansion of the time-variable mean anomaly:

$$M(t) = M(t_0) + n(t - t_0) + \Delta M_d (t - t_0)^2, \tag{1}$$

where

$$\Delta M_d = \frac{1}{2}\dot{n}, \tag{2}$$

where n is the mean motion, t is the time, and t_0 is the epoch. ΔM_d was stepped from -15 to $+15$ deg/yr^2 in case of 1999 KW4 and from -9 to $+39$ deg/yr^2 in case

of 2001 SL9 and all other parameters were fitted at each step. [1]

To reduce the complexity of the model, we estimated upper limits on the eccentricity of the mutual orbits by fitting the data from the best covered apparitions: the 2001 apparition for 1999 KW4 and the 2013 apparition for 2001 SL9. The model includes a precession of the line of apsides. The pericenter drift rate depends on the polar flattening of the primary (see Murray and Dermott, 1999, Eq. (6.249)), but as the polar flattenings are poorly constrained from the data (see Tables 4 and 5), we instead fit the drift rate as an independent parameter. Its initial values were stepped in a range from zero to 25°/day. This range encompassed all plausible values for the flattening of the primaries and other parameters of the systems.

Since we found that the upper limits on eccentricity were low, in further modeling of the data from all apparitions together, we set the eccentricity equal to zero for simplicity and efficiency. This assumption had a negligible effect on the accuracy of other derived parameters of the models.

Across all observations, we found a unique solution for the system parameters except for an ambiguity in the quadratic drift in mean anomaly and the orbital period of 2001 SL9, see Tables 4 and 5. We describe and discuss these parameters in Sections 3 and 4. Plots of the RMS residuals vs ΔM_d are shown in Figs. 1 and 2. In order to save computing time, the plots were constructed using spherical shapes of both components. However, neighborhoods of local minima were then revisited using elipsoidal shapes in order to improve the fit.

For 1999 KW4, RMS residuals of the two best local minima obtained using the spherical shapes (with ΔM_d of -0.65 and -5.8 deg/yr^2) were 0.0355 and 0.0385 mag, respectively. The fits improved to 0.0301 and 0.0359 mag using the elipsoidal shapes. The fit is significanly poorer for the latter solution. The former solution provides a satisfactory fit to the data and it is accepted as real solution for the binary asteroid parameters.

For 2001 SL9, RMS residuals of the five best local minima obtained using the spherical shapes (with ΔM_d of 2.8, 5.2, 7.6, 4.0 and 0.5 deg/yr^2) were 0.0238. 0.0238, 0.0245, 0.0246 and 0.0248 mag, respectively. The fits improved to 0.0236, 0.0236, 0.0243, 0.0245 and 0.0245 mag using the elipsoidal shapes; the marginal improvement is due to that the secondary of 2001 SL9 is not prominently elongated. The first two solution provide satisfactory fit to the data; one of them is a real solution for the binary asteroid parameters, but we cannot resolve this ambiguity with the available data. The other three solutions with the higher RMS residuals provide significantly poorer fits to the data and they do not appear real.

Figures 4 and 8 show the quadratic drift in the mean anomaly with respect to a solution with constant orbital period. Examples of the long-period component data

[1] ΔM_d of 2001 SL9 was sampled on the larger interval because in our initial modeling runs, there appeared possible solutions at high positive ΔM_d values. Therefore, we expanded the interval in order to examine them; there turned out no significant solutions at high ΔM_d finally.

together with the synthetic lightcurves of the best-fit solutions are presented in Figs. 3 and 7. Uncertainty areas of the orbital poles are shown in Figs. 5 and 9.

We estimated realistic uncertainties of the fitted parameters using the procedure described in Scheirich and Pravec (2009). For each parameter, we obtained its admissible range that corresponds to a 3-σ uncertainty.

3 Parameters of (66391) 1999 KW4

In this section, we summarize the best-fit model parameters of the binary system (66391) 1999 KW4 and overview previous publications. The parameters are listed in Table 4.

In the first part of the table, we present data derived from optical and spectroscopic observations of the system. H_V and G are the mean absolute magnitude and the phase parameter of the H–G phase relation (Bowell et al., 1989). $p_{\rm V}$ is the visual geometric albedo.

XXXX - spectral class: Appendix.

In the next two parts of Table 4, we give parameters for the components of the binary. The indices 1 and 2 refer to the primary and the secondary, respectively.

$D_{i,{\rm C}}$ is the cross-section equivalent diameter, i.e., the diameter of a sphere with the same cross section, of the i-th component at the observed aspect. Since the aspect is changing over time, the given value is an average over all lightcurve sessions. To quantify the mean aspect we used an asterocentric latitude of a Phase Angle Bisector (PAB), which is the mean direction between the heliocentric and geocentric directions to the asteroid. As discussed in Harris et al. (1984), this is an approximation for the effective viewing direction of an asteroid observed at non-zero solar phase. The average absolute value of the asterocentric latitude of the PAB (computed using the nominal pole of the mutual orbit, assumed to be the rotational pole of both components) was 27 deg.

$D_{i,{\rm V}}$ is the volume equivalent diameter, i.e., the diameter of a sphere with the same volume, of the i-th component.

$D_{2,{\rm C}}/D_{1,{\rm C}}$ is the ratio between the cross-section equivalent diameters of the components. P_i is the rotational period of the i-th component.

An analysis of the best subset of data for the secondary rotation taken from 2018-06-07.9 to -11.0 gave a formal best-fit estimate for the secondary rotation period of 17.53 ± 0.12 (3σ; this includes also a synodic-sidereal difference uncertainty). This agrees with the mutual orbit period, within the error bar. Considering that all the observed secondary lightcurve minima coincide with or lie close to the mutual events —small differences may be due to a phase effect or secondary libration—, it is very likely that the secondary is in synchronous rotation. We therefore assume that P_2 is equal to the orbital period (see Table 4).

$(A_1B_1)^{1/2}/C_1$ is a ratio between the mean equatorial and the polar axes of the primary. A_i/B_i is a ratio between the equatorial axes of the i-th component (equatorial elongation). $\rho_1 = \rho_2$ are the bulk densities of the two components, which we assumed to be the same in our modeling.

Most of the quantities were parameters of our model given in Section 2.2 and we derived them from our observations.

Table 4
Properties of binary asteroid (66391) 1999 KW4.

Parameter	Value	Unc.	Reference
Whole system:			
H_V	16.74 ± 0.22	1σ	This work
G	$(0.24 \pm 0.11)^a$	1σ	This work
$p_{\rm V}$	0.162 ± 0.034	1σ	This work
Taxon. class	Q		This work
Primary:			
$D_{1,\rm C}$ (km)	1.367 ± 0.041^b	1σ	From O06
$D_{1,\rm V}$ (km)	1.317 ± 0.040	1σ	O06
P_1 (h)	2.7645 ± 0.0003	1σ	O06
$(A_1B_1)^{1/2}/C_1$	$\leq 1.6^c$ / 1.17 ± 0.15	3σ	This work / O06
A_1/B_1	1.04 ± 0.04	1σ	O06
ρ_1 (g cm^{-3})	$1.3^{+0.7}_{-0.4}$ / 1.97 ± 0.72	3σ	This work / O06
Secondary:			
$D_{2,\rm C}/D_{1,\rm C}$	0.42 ± 0.03^d	3σ	This work
$D_{2,\rm C}$ (km)	0.574 ± 0.066	3σ	This work
$D_{2,\rm V}$ (km)	$(0.59 \pm 0.04)^e$	1σ	This work
P_2 (h)	$(17.46)^f$		This work
A_2/B_2	$1.3^{+0.3}_{-0.1}$	3σ	This work
Mutual orbit:			
$a/(A_1B_1)^{1/2}$	1.7 ± 0.2	3σ	This work
$(L_{\rm P}, B_{\rm P})$ (deg.)	$(329.6, -62.3) \pm (12 \times 4)^g$	3σ	This work
$P_{\rm orb}$ (h)	17.45758 ± 0.00004^h	3σ	This work
e	≤ 0.006	3σ	O06
ΔM_d (deg/yr^2)	-0.65 ± 0.15	3σ	This work
$\dot{P}_{\rm orb}$ (h/yr)	0.00013 ± 0.00003	3σ	This work
$\dot{a}$ (cm/yr)	1.2 ± 0.3	3σ	This work

References: O06 (Ostro et al., 2006)

[a] The range of high solar phase angles covered by the observations did not allow to determine the G parameter. We assumed the mean G value for S-complex asteroids (Warner et al., 2009).

[b] Derived from the primary shape model by O06 and for the average observed aspect. See text for details.

[c] The formal best-fit value is 1.1.

[d] This is a ratio of the cross-section equivalent diameters for the average observed aspect. See text for details.

[e] Derived using the shape model of the secondary from O06 rescaled by 130%. See text for details.

[f] The secondary appears to be in synchronous rotation. See text for details.

[g] These are the semiaxes of the uncertainty area; see its actual shape in Fig. 5.

[h] The $P_{\rm orb}$ value for epoch JD 2455242.86, for which $P_{\rm orb}$ and ΔM_d do not correlate.

The cross-section and volume equivalent diameters of the primary were derived using the shape model of the primary from Ostro et al. (2006). Assuming its rotational pole is the same as the mutual orbital pole (see below), we computed its rotationally averaged cross-section for each lightcurve session and presented the mean value over all sessions. Its 1σ uncertainty was computed using the uncertainties of the dimensions of the primary from Ostro et al.

$D_{1,\mathrm{V}}$ was taken from Table 2 of Ostro et al.

$D_{2,\mathrm{V}}$ was derived using the shape model of the secondary by Ostro et al. (2006), rescaled to 130% of its original size to match mutual events' depths from our data (see below). Its 1σ uncertainty is a formal value taken from Table 2 of Ostro et al. (2006), but the real uncertainty may be higher because of uncertainties of the secondary radar shape model (Lance Benner, personal communication).

In the last part of Table 4, we summarize the parameters of the mutual orbit of the binary components. a is the semimajor axis, $L_\mathrm{P}, B_\mathrm{P}$ are the ecliptic coordinates of the orbital pole in the equinox J2000, e is the orbit eccentricity (only the upper limit was derived), and ΔM_d is the quadratic drift in mean anomaly. Since the orbital period P_orb is changing in time, the value presented in Table 4 is valid for epoch JD 2455242.86. For this epoch, which is approximately the mean time of all observed events, a correlation between P_orb and ΔM_d is zero. We also give the time derivatives of the orbital period and the semimajor axis, derived from ΔM_d.

Although the orbit of 1999 KW4 crosses those of Earth, Venus and Mercury, according to JPL HORIZONS system the asteroid experienced only four close approaches to Earth between 2000 and 2019. The approaches took place in May 2001, May 2002, May 2018 and May 2019 at distances of 0.032, 0.089, 0.078 and 0.035 AU, respectively. Since the observed mutual orbital period increase is based on the observations at six effective epochs (apparitions), we can rule out planetary-tug effects as a potential mechanism for the increase.

The uncertainty area of the orbital pole is shown in Fig. 5. The size of the area shrinks with increasing the flattening of the primary $(A_1B_1)^{1/2}/C_1$. To demonstrate the effect, we constrained the orbital pole uncertainties using three fixed values of the flattening (1.0, 1.2 and 1.4) and plotted the respective areas in the figure.

The uncertainties of the mutual semimajor axis and flattening of the primary are the main sources of the uncertainty of the bulk density of the system. In addition to that, the uncertainties of the two parameters are not independent. We therefore stepped a and $(A_1B_1)^{1/2}/C_1$ on a grid (while all other parameters were fitted at each step) to obtain an uncertainty area of both parameters together. The area is shown in Fig. 6 with values of the bulk density for each combination of the parameters indicated.

The mutual orbit and shapes of the binary asteroid components of 1999 KW4 were modeled by Ostro et al. (2006) with radar observations taken in 2001. They report the size of the primary to be close to a tri-axial ellipsoid with axes 1417 $\times$ 1361 $\times$ 1183 m (1σ uncertainties of $\pm$ 3%), and the secondary to be a tri-axial ellipsoid

with axes 595 × 450 × 343 m (1σ uncertainties of ± 5%). The dimensions given are extents of dynamically equivalent equal-volume ellipsoid (DEEVE; a homogeneous ellipsoid having the same moment-of-inertia ratios and volume as the shape model).

They also found the parameters of the mutual orbit to be as following: orbital period $P_{\rm orb} = 17.422 \pm 0.036$ h, semimajor axis $a = 2548 \pm 15$ m, eccentricity $e = 0.0004 \pm 0.0019$, pole direction in ecliptic coordinates: $L_{\rm P} = 325.8 \pm 3.5$ deg, $B_{\rm P} = -61.8 \pm 1.2$ deg (uncertainties correspond to 1σ).

To compare our results with the values from Ostro et al. (2006), we computed $(A_1B_1)^{1/2}/C_1$ and $a/(A_1B_1)^{1/2}$ using their DEEVE for the primary and their semimajor axis of the mutual orbit. The result is plotted as a solid point in Fig. 6 with 1σ error bars.

There is one significant discrepancy between our results and those by Ostro et al. (2006): We obtained a significantly larger secondary-to-primary size ratio. To compare their result with our, we computed a mean (rotationally averaged) cross-section ratio from the component shapes by Ostro et al. (2006): $(D_{2,\rm C}/D_{1,\rm C})_{\rm radar} = 0.34 \pm 0.02$ (1σ) at the same mean aspect as our observations (asterocentric latitude of the Phase Angle Bisector, $B_{\rm PAB} = 27$ deg). The value is significantly lower than our $D_{2,\rm C}/D_{1,\rm C} = 0.42 \pm 0.03$ (3σ).

To look more into the discrepancy between the secondary-to-primary size ratios by Ostro et al. (2006) and by us, we performed following test. Using the shape models of both components from Ostro et al. and the orbital parameters from Table 4, we generated a synthetic long-period component of the lightcurve. We then increased the size of the secondary until the depths of the secondary events (occultations and eclipses of the secondary) matched the observed event depths. We obtained a match when we increased the secondary axes by Ostro et al. (2006) to 130% of their original values. This is even slightly greater than $0.42/0.34 \doteq 124\%$ because in this test the actual light scattering model was used for calculating the synthetic lightcurve, which models the scattering from non-spherical component shapes at the high solar phases and it is more precise than simply comparing the estimated mean cross-sections above. We note that replacing the parameters of the mutual orbit with those derived by Ostro et al. did not change the result.

We discussed this issue with Lance Benner and we received following information: "The dimensions of the secondary might be underestimated by Ostro et al. (2006) because the radar images were obtained at relatively coarse range and Doppler resolutions and at modest signal-to-noise ratios. Consequently, it is plausible that the trailing edge of the secondary in the radar images images were less than would be detected if the SNRs were substantially higher." (Lance Benner, personal communication.)

4 Parameters of (88710) 2001 SL9

In this section, we summarize the best-fit model parameters of the binary system (88710) 2001 SL9 and overview previous publications. The parameters are listed in Table 5.

The notation of the values in the table and their uncertainties are the same as in Table 4 (see Section 3).

The average absolute value of the asterocentric latitude of the PAB (computed using the nominal pole of the mutual orbit, assumed to be the rotation pole of both components) was 11 deg; we observed the asteroid close to equator-on.

Two works were published reporting spectroscopic observations of 2001 SL9 in the visual and near-infrared spectral range: Lazzarin et al., 2004 and 2005. Based on moderate slope and broad 1μm and 2μm absorbtion bands they classified 2001 SL9 as an Sr and Q type asteroid, respectively. The Q class is preferred, as the Sr classification was based on the visual spectra only, while the Q class was derived from spectral observations covering the visual to the near-infrared range. From the measured H_V and assuming the mean albedo for S-complex asteroids (Pravec et al., 2012), we estimated the effective diameter of the system $D_{\rm eff}$ at the observed (near equator-on) aspect.

A rotational state of the secondary is particularly important for the interpretations we present in Section 5. However, as an amplitude of secondary rotation lightcurve is very low, we could not derive its rotation period from the available data. It appears that the secondary is nearly spheroidal with low equatorial elongation.

Pravec et al. (2016) showed that asynchronous secondaries are absent among observed binary systems with closest orbits ($a/D_1 \lesssim 2.2$, $P_{\rm orb} \lesssim 20$ h). They also pointed out that asynchronous secondaries are typically observed on eccentric orbits. Based on that, the parameters of the mutual orbit of 2001 SL9 (a close orbit with low or zero eccentricity) and the fact that the secondary spin relaxation is typically much faster than the orbit circularization (Goldreich and Sari, 2009), we assume that the secondary of 2001 SL9 is in synchronous rotation, i.e., its rotation period is the same as the orbit period.

Earlier work where some of the binary parameters were derived is Pravec et al. (2006). Their values are generally in agreement with our current best estimated parameters, but they did not perform a modeling in order to get parametes of the mutual orbit.

The binary (88710) 2001 SL9 appears to be a typical near-Earth binary asteroid according to its basic parameters. Its bulk density of ~ 1.8 g cm^{-3} is in good agreement with its rocky taxonomical class. The normalized total angular momentum content of 2001 SL9 is XXXX $\alpha_L = 1.1 \pm 0.2$ (1-σ uncertainty), i.e., in the range 0.9–1.3 for small near-Earth and main belt asteroid binaries and exactly as expected for the proposed formation of small binary asteroids by fission of critically spinning

Table 5
Properties of binary asteroid (88710) 2001 SL9.

Parameter	Value	Unc.	Reference
Whole system:			
H_V	17.98 ± 0.02	1σ	This work
G	0.34 ± 0.03	1σ	This work
$V-R$	0.457 ± 0.010	1σ	This work
$D_{\rm eff}$ (km)	0.75 ± 0.10^a	1σ	This work
Taxon. class	Q		L05
Primary:			
$D_{1,\rm C}$ (km)	0.73 ± 0.32	3σ	This work
$D_{1,\rm V}$ (km)	0.77 ± 0.34	3σ	This work
P_1 (h)	2.4004 ± 0.0002	1σ	P06
$(A_1B_1)^{1/2}/C_1$	$\leq 2.2^b$	3σ	This work
A_1/B_1	1.07 ± 0.01	1σ	PH07
$\rho_1 = \rho_2$ (g cm^{-3})	$1.8^{+2.5}_{-0.5}$	3σ	This work
Secondary:			
$D_{2,\rm C}/D_{1,\rm C}$	0.24 ± 0.02	3σ	This work
$D_{2,\rm C}$ (km)	0.18 ± 0.08	3σ	This work
$D_{2,\rm V}$ (km)	$(0.18 \pm 0.08)^c$	3σ	This work
P_2 (h)	$(16.40)^d$		
A_2/B_2	≤ 1.2	3σ	This work
Mutual orbit:			
$a/(A_1B_1)^{1/2}$	1.75 ± 0.3	3σ	This work
$(L_{\rm P}, B_{\rm P})$ (deg.)	$(302, -73) \pm (10 \times 4)^e$	3σ	This work
$P_{\rm orb}$ (h)	16.4022 ± 0.0002^f	3σ	This work
	16.4027 ± 0.0002^f		
e	≤ 0.07	3σ	This work
ΔM_d (deg/yr^2)	2.8 ± 0.2	3σ	This work
	5.2 ± 0.2		
$\dot{P}_{\rm orb}$ (h/yr)	-0.00048 ± 0.00003	3σ	This work
	-0.00089 ± 0.00004		
$\dot{a}$ (cm/yr)	-2.8 ± 0.2	3σ	This work
	-5.1 ± 0.2		

References: P06 (Pravec et al., 2006), PH07 (Pravec and Harris, 2007), L05 (Lazzarin et al., 2005).
[a] From the derived H_V and assumed $p_V = 0.20 \pm 0.05$ that is the mean albedo for S-complex asteroids (Pravec et al., 2012).
[b] The formal best-fit value is 1.7.
[c] Assuming a spherical shape of the secondary.
[d] The secondary is assumed to in synchronous rotation. See text for details.
[e] These are the semiaxes of the uncertainty area; see its actual shape in Fig. 9.
[f] These are the periods of the two solutions of ΔM_d for epoch 2012-09-12.

rubble-pile progenitors (Pravec and Harris, 2007).

According to JPL HORIZONS system, the closest Earth, Venus and Mars approaches of 2001 SL9 from 2001 to 2015 were 0.22, 0.13 and 0.36 AU, respectively. We can therefore rule out planetary-tug effects as a potential mechanism for the observed mutual orbital period decrese.

5 Implications for the BYORP effect

XXXX

6 Conclusions

XXXX

Acknowledgements

XXXX

References

Benner, L.A.M., Ostro, S.J., Giorgini, J.D., Jurgens, R.F., Margot, J.-L., Nolan, M.C., 2001. 1999 KW4. IAU Circ. 7632.

Binzel et al., Icarus 170, 259 (2004).

Bottke, Jr., W. F., Vokrouhlický, D., Rubincam, D. P., Nesvorný, D., 2006. The Yarkovsky and Yorp Effects: Implications for Asteroid Dynamics. Annual Review of Earth and Planetary Sciences, 34, 157–191.

Bowell, E., Hapke, B., Domingue, D., Lumme, K., Peltoniemi, J., Harris, A.W., 1989. Application of photometric models to asteroids. In: Asteroids II. Univ. Arizona Press, pp. 524-556.

Chesley, S. R., Ostro, S. J., Vokrouhlický, D., Čapek, D., Giorgini, J. D., Nolan, M. C., Margot, J.-L., Hine, A. A., Benner, L. A. M., Chamberlin, A. B., 2003. Direct Detection of the Yarkovsky Effect by Radar Ranging to Asteroid 6489 Golevka. Science, 302, 1739–1742.

Ćuk, M., Burns, J.A., 2005. Effects of thermal radiation on the dynamics of binary NEAs. Icarus, 176, 418–431.

Goldreich, P., Sari, R., 2009. Tidal Evolution of Rubble Piles. Astroph. Journal, 691, 54–60.

Harris, A.W., Young, J.W., Scaltriti, F., Zappalà, V., 1984. Lightcurves and phase relations of the Asteroids 82 Alkmene and 444 Gyptis. Icarus 57, 251258.

Jacobson, S.A., Scheeres, D.J., 2011. Long-term Stable Equilibria for Synchronous Binary Asteroids. ApJ Letters, 736, L19.

Kaasalainen, M., Mottola, S., Fulchignoni, M., 2002. Asteroid Models from Disk-integrated Data. In Asteroids III, ed. W. F. Bottke Jr., A. Cellino, P. Paolicchi, R.

P. Binzel, University of Arizona Press, Tucson, pp. 139.

Kaasalainen, M., Ďurech, J., Warner, B. D., Krugly, Y. N., Gaftonyuk, N. M., 2007. Acceleration of the rotation of asteroid 1862 Apollo by radiation torques. Nature, 446, 420-422.

Lazzarin, M., Marchi, S., Barucci, M. A., Di Martino, M., Barbieri, C., 2004. Visible and near-infrared spectroscopic investigation of near-Earth objects at ESO: first results. Icarus, 169, 373–384

Lazzarin, M., Marchi, S., Magrin, S., Licandro, J., 2005. Spectroscopic investigation of near-Earth objects at Telescopio Nazionale Galileo. Monthly Notices of the Royal Astronomical Society, 359, 1575–1582

Lowry, S. C., Fitzsimmons, A., Pravec, P., Vokrouhlický, D., Boehnhardt, H., Taylor, P. A., Margot, J.-L., Galád, A., Irwin, M., Irwin, J., Kusnirák, P., 2007. Direct Detection of the Asteroidal YORP Effect. Science, 316, 272–274.

McMahon, J., Scheeres, D., 2010a. Secular orbit variation due to solar radiation effects: a detailed model for BYORP. Celestial Mechanics and Dynamical Astronomy, 106, 261–300.

McMahon, J., Scheeres, D., 2010b. Detailed prediction for the BYORP effect on binary near-Earth Asteroid (66391) 1999 KW4 and implications for the binary population. Icarus, 209, 494–509.

Murray, C.D., Dermott, S.F., 1999. Solar System Dynamics. Cambridge University Press.

Ostro, S.J., Margot, J.-L., Benner, L.A.M., Giorgini, J.D., Scheeres, D.J., Fahnestock, E.G., Broschart, S.B., Bellerose, J., Nolan, M.C., Magri, C., Pravec, P., Scheirich, P., Rose, R., Jurgens, R.F., De Jong, E.M., Suzuki, S., 2006. Radar Imaging of Binary Near-Earth Asteroid (66391) 1999 KW4. Science, 314, 1276–1280.

Pravec, P., Kušnirák, P., Warner, B., 2001. 2001 SL9. IAUC 7742.

Pravec, P., Scheirich, P., Kušnirák, P., Šarounová, L., Mottola, S., Hahn, G., Brown, P., Esquerdo, G., Kaiser, N., Krzeminski, Z., Pray, D.P., Warner, B.D., Harris, A.W., Nolan, M.C., Howell, E.S., Benner, L.A. M., Margot, J.-L., Galád, A., Holliday, W., Hicks, M.D., Krugly, Yu.N., Tholen, D., Whiteley, R., Marchis, F., Degraff, D.R., Grauer, A., Larson, S., Velichko, F.P., Cooney, W.R., Stephens, R., Zhu, J., Kirsch, K., Dyvig, R., Snyder, L., Reddy, V., Moore, S., Gajdoš, Š., Világi, J., Masi, G., Higgins, D., Funkhouser, G., Knight, B., Slivan, S., Behrend, R., Grenon, M., Burki, G., Roy, R., Demeautis, C., Matter, D., Waelchli, N., Revaz, Y., Klotz, A., Rieugné, M., Thierry, P., Cotrez, V., Brunetto, L., Kober, G., 2006. Photometric survey of binary near-Earth asteroids. Icarus, 181, 63–93.

Pravec, P., Harris, A.W., 2007. Binary asteroid population. 1: Angular momentum content. Icarus 190, 250-259.

Pravec, P., Scheirich, P., 2010. Binary System Candidates for Detection of BY-ORP. 42nd annual meeting of the Division for Planetary Sciences of the American Astronomical Society, Oct. 3 - Oct. 8, 2010, Pasadena, CA.

Pravec, P., Harris, A.W., Kušnirák, P., Galád, A., Hornoch, K. 2012. Absolute magnitudes of asteroids and a revision of asteroid albedo estimates from WISE thermal observations. Icarus 221, 365-387.

Pravec, P., Scheirich, P., Kušnirák, P., Hornoch, K., Galád, A., Naidu, S. P., Pray, D. P., Világi, J., Gajdoš, Š., Kornoš, L., Krugly, Y. N., Cooney, W. R., Gross, J., Terrell, D., Gaftonyuk, N., Pollock, J., Husárik, M., Chiorny, V., Stephens, R. D., Durkee, R., Reddy, V., Dyvig, R., Vraštil, J., Žižka, J., Mottola, S., Hellmich, S., Oey, J., Benishek, V., Kryszczyńska, A., Higgins, D., Ries, J., Marchis, F., Baek, M., Macomber, B., Inasaridze, R., Kvaratskhelia, O., Ayvazian, V., Rumyantsev, V., Masi, G., Colas, F., Lecacheux, J., Montaigut, R., Leroy, A., Brown, P., Krzeminski, Z., Molotov, I., Reichart, D., Haislip, J., LaCluyze, A., 2016. Binary asteroid population. 3. Secondary rotations and elongations. Icarus, 267, 267–295.

Scheirich, P., Pravec, P., 2009. Modeling of lightcurves of binary asteroids. Icarus, 200, 531–547.

Scheirich, P., Pravec, P., Jacobson, S. A., Ďurech, J., Kušnirák, P., Hornoch, K., Mottola, S., Mommert, M., Hellmich, S., Pray, D., Polishook, D., Krugly, Y. N., Inasaridze, R. Y., Kvaratskhelia, O. I., Ayvazian, V., Slyusarev, I., Pittichová, J., Jehin, E., Manfroid, J., Gillon, M., Galád, A., Pollock, J., Licandro, J., Alí-Lagoa, V., Brinsfield, J., Molotov, I. E., 2015. The binary near-Earth Asteroid (175706) 1996 FG_3 – An observational constraint on its orbital evolution. Icarus, 245, 56–63.

Steinberg, E., Sari, R., 2011. Binary YORP Effect and Evolution of Binary Asteroids. Astronomical Journal, 141, 55–65

Taylor, P. A., Margot, J.-L., Vokrouhlický, D., Scheeres, D. J., Pravec, P., Lowry, S. C., Fitzsimmons, A., Nolan, M. C., Ostro, S. J., Benner, L. A. M., Giorgini, J. D., Magri, C., 2007. Spin Rate of Asteroid (54509) 2000 PH5 Increasing Due to the YORP Effect. Science, 316, 274–277.

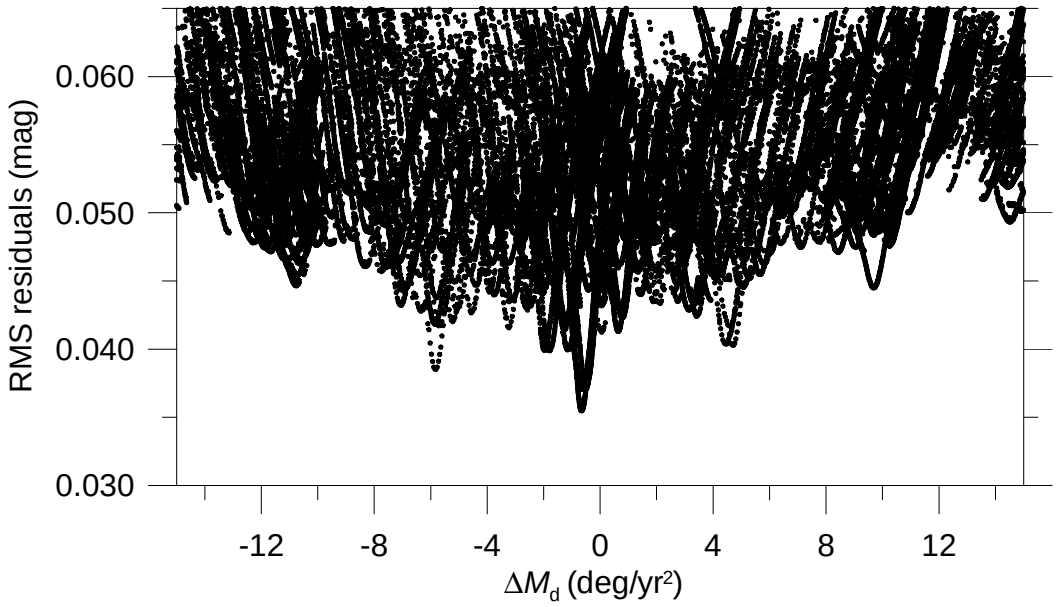

Fig. 1. The RMS residuals vs. ΔM_d for solutions of the model of (66391) 1999 KW4 presented in Section 2.2. Each dot represents the best-fit result with ΔM_d fixed and other parameters varied. The plots were constructed using spherical shapes of both components; see text for details.

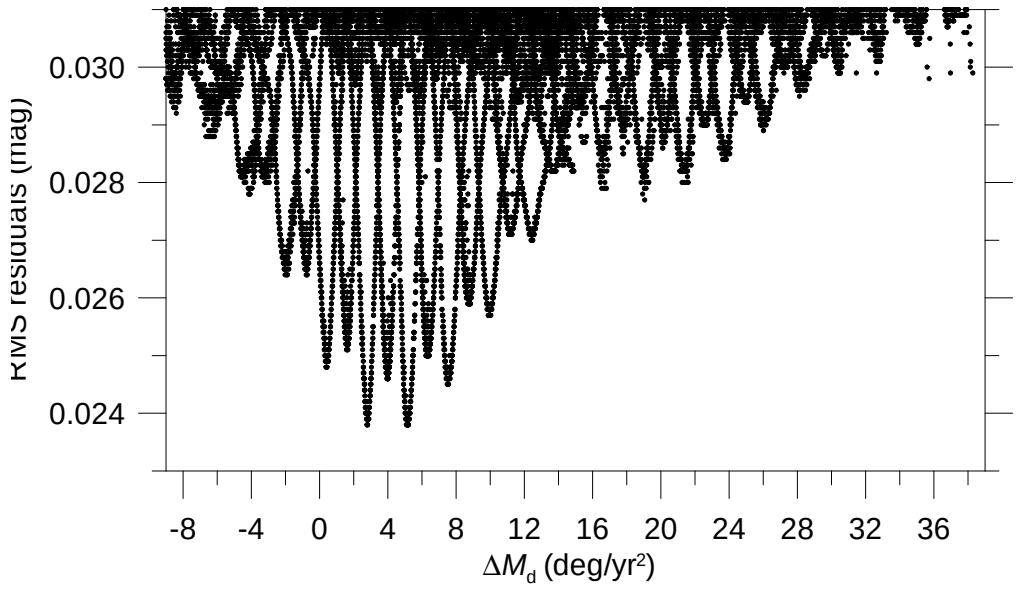

Fig. 2. The RMS residuals vs. ΔM_d for solutions of the model of (88710) 2001 SL9 presented in Section 2.2. Each dot represents the best-fit result with ΔM_d fixed and other parameters varied. The plots were constructed using spherical shapes of both components; see text for details.

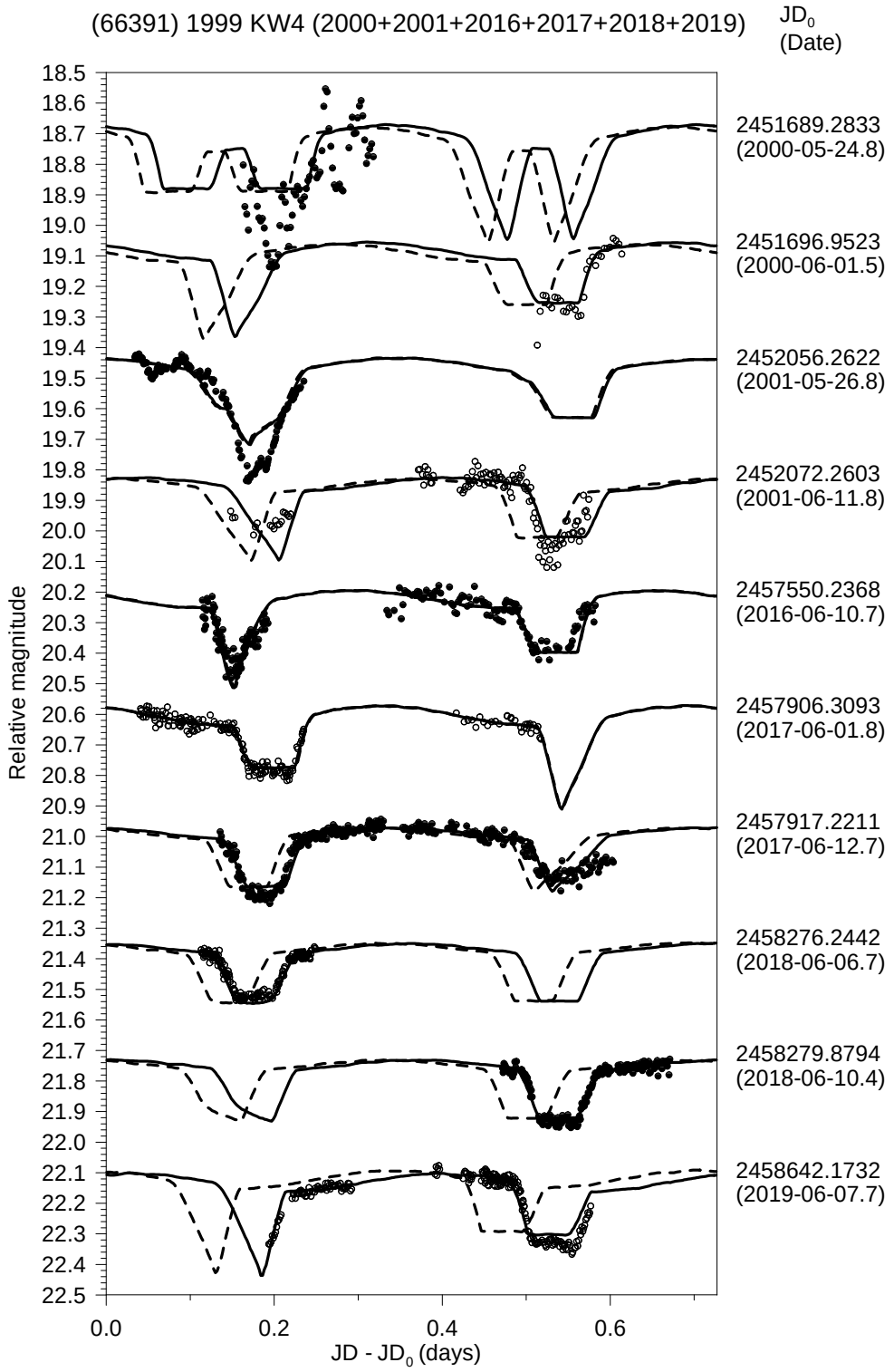

Fig. 3. Selected data of the long-period lightcurve component of (66391) 1999 KW4. The observed data are marked as points. The solid curve represents the synthetic lightcurve for the best-fit solution with $\Delta M_d = -0.65$ deg/yr^2. For comparison, the dashed curve is for the best-fit model with ΔM_d fixed at 0.0 deg/yr^2.

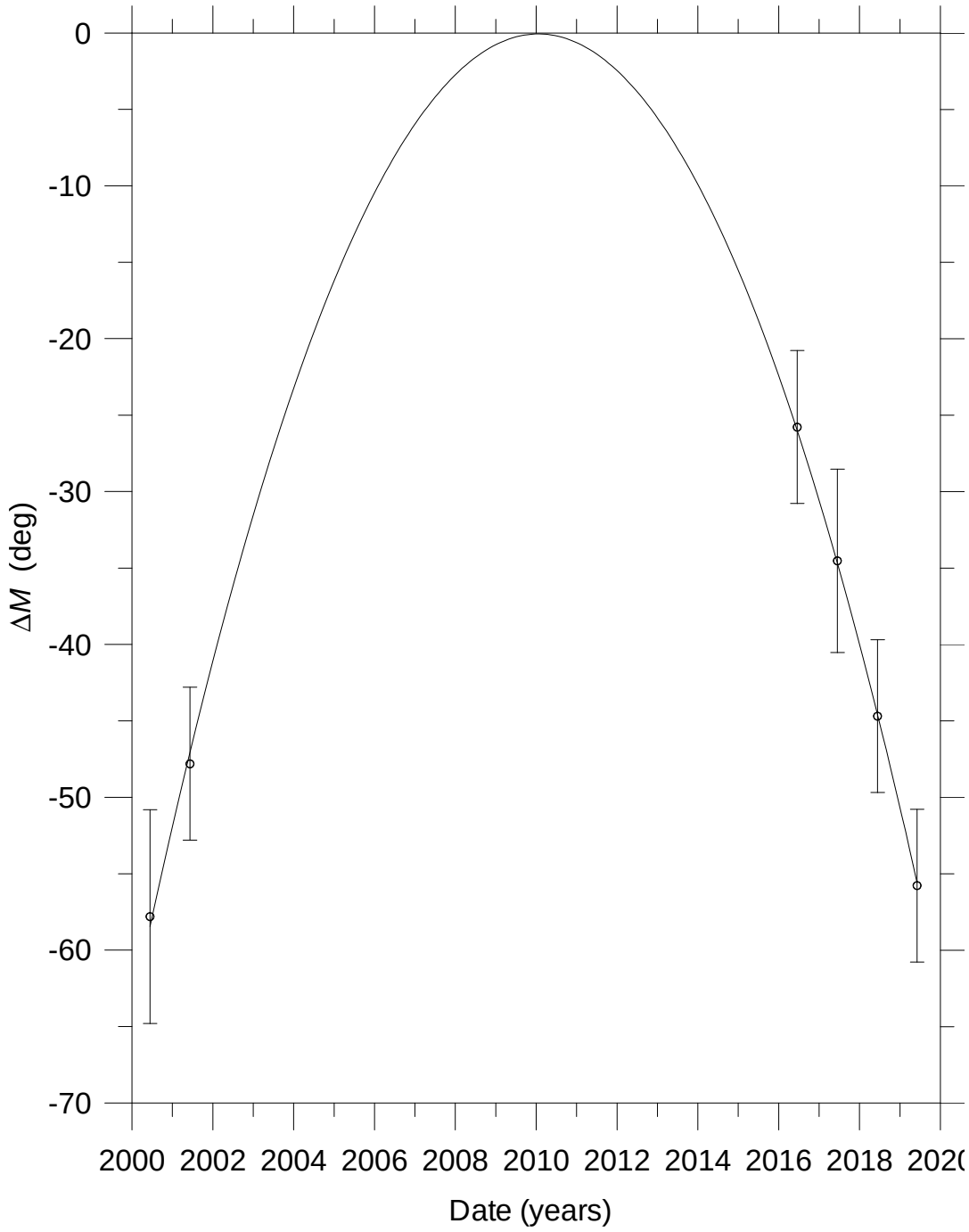

Fig. 4. A time evolution of the mean anomaly difference ΔM between the best-fit solution with a constant orbital period (i.e., with ΔM_d fixed at zero) and the best-fit solution with ΔM_d fitted for (66391) 1999 KW4. Each point corresponds to the middle of one of the six apparitions from 2000 to 2019. Vertical error bars represent estimated 3σ uncertainties of the event timess, expressed in mean anomaly. The solid line is a quadratic fit to the data points.

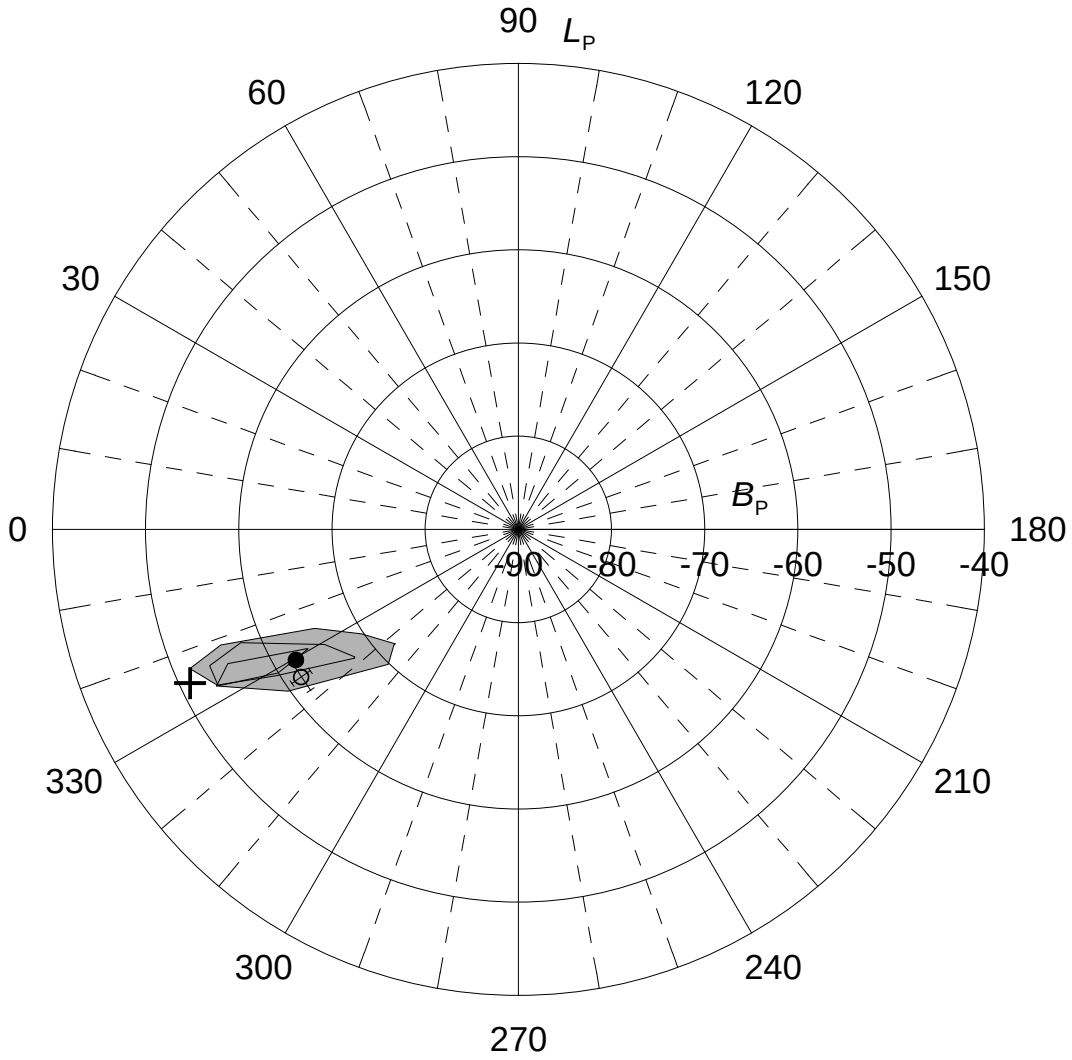

Fig. 5. Area of admissible poles for the mutual orbit of (66391) 1999 KW4 in ecliptic coordinates (grey area) for $(A_1B_1)^{1/2}/C_1 = 1$. The dot is the nominal solution given in Table 4. This area corresponds to 3σ confidence level. To demonstrate the effect of a flattening of the primary on the estimated pole, the areas confined by solid lines shows the admissible poles constrained using $(A_1B_1)^{1/2}/C_1 = 1.2$ (middle area) and 1.4 (the smallest area). The open circle with error bars represents a solution for orbital pole from Ostro et al. 2006 with 1σ uncertainties. The south pole of the current asteroid's heliocentric orbit is marked with the cross.

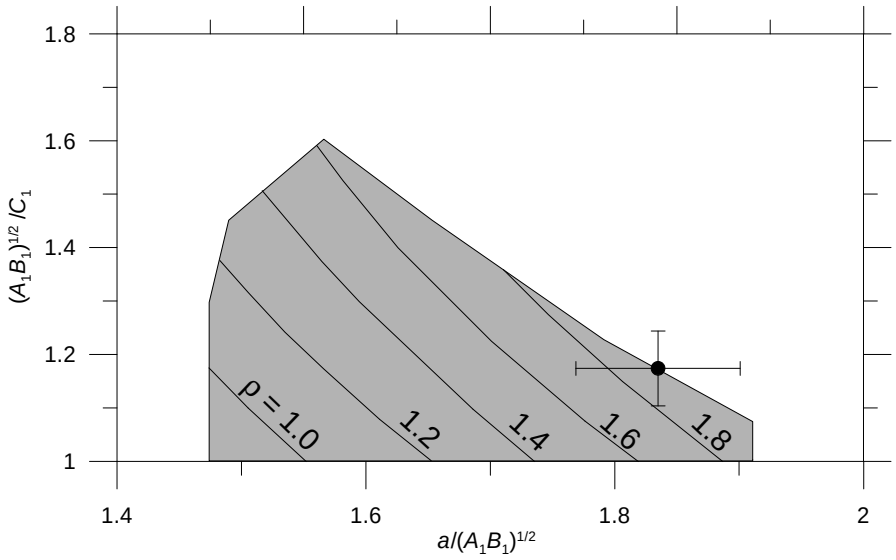

Fig. 6. Area of admissible combinations of the ratio between the mean equatorial and the polar axes of the primary ($(A_1B_1)^{1/2}/C_1$) and the semimajor axis of the mutual orbit a of (66391) 1999 KW4. This area corresponds to 3σ confidence level. Values of the bulk density of the system (ρ) in g cm^{-3} are indicated. The dot with the error bars is the result from Ostro et al. (2006) and its 1σ uncertainties (see text for details).

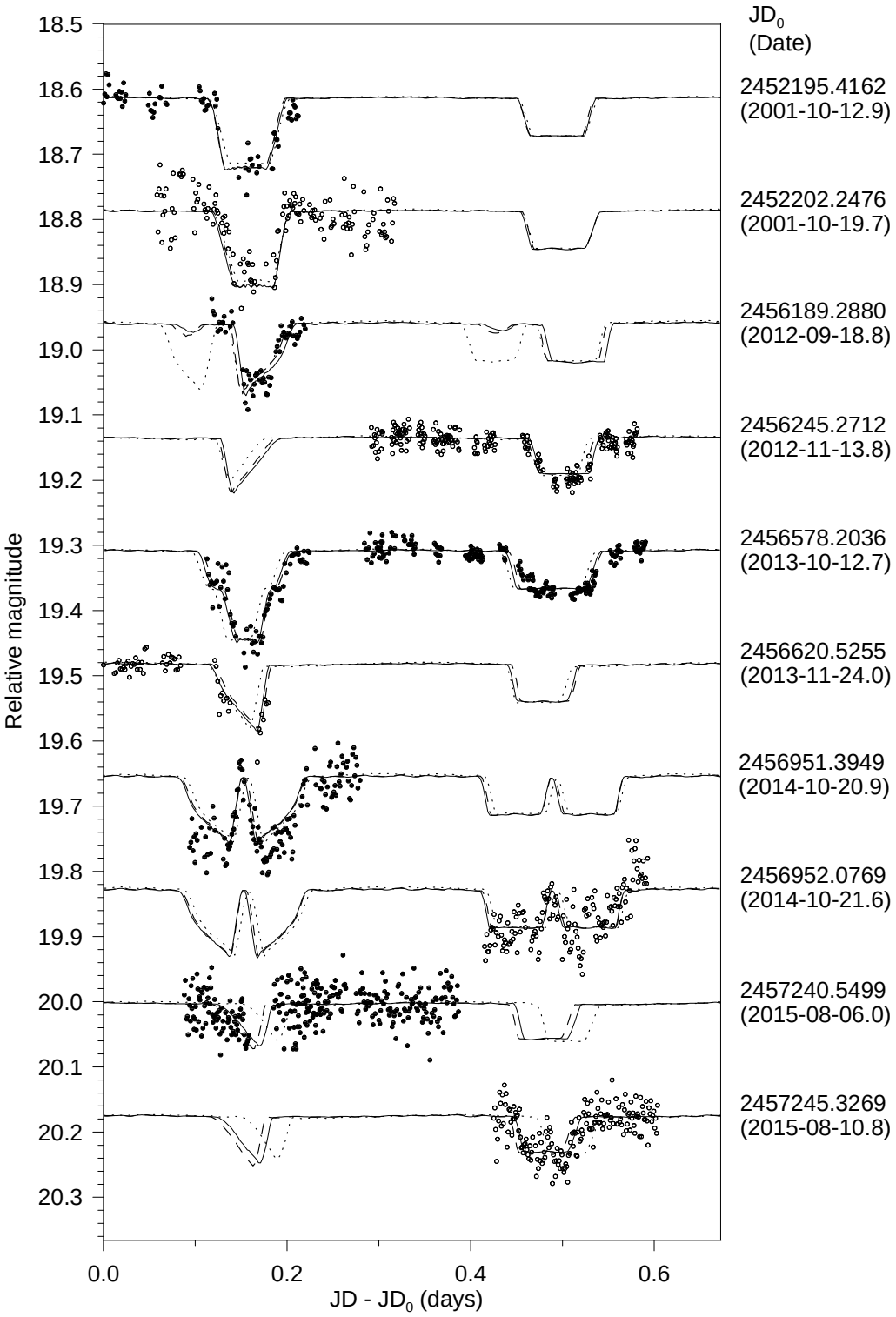

Fig. 7. Selected data of the long-period lightcurve component of 2001 SL9. The observed data are marked as points. The solid and dashed curves represent the synthetic lightcurves of the two best-fit solutions with $\Delta M_d = 2.8$ and 5.2 deg/yr^2, respectively. For comparison, the dotted curve is for the best-fit model with ΔM_d fixed at 0.0 deg/yr^2.

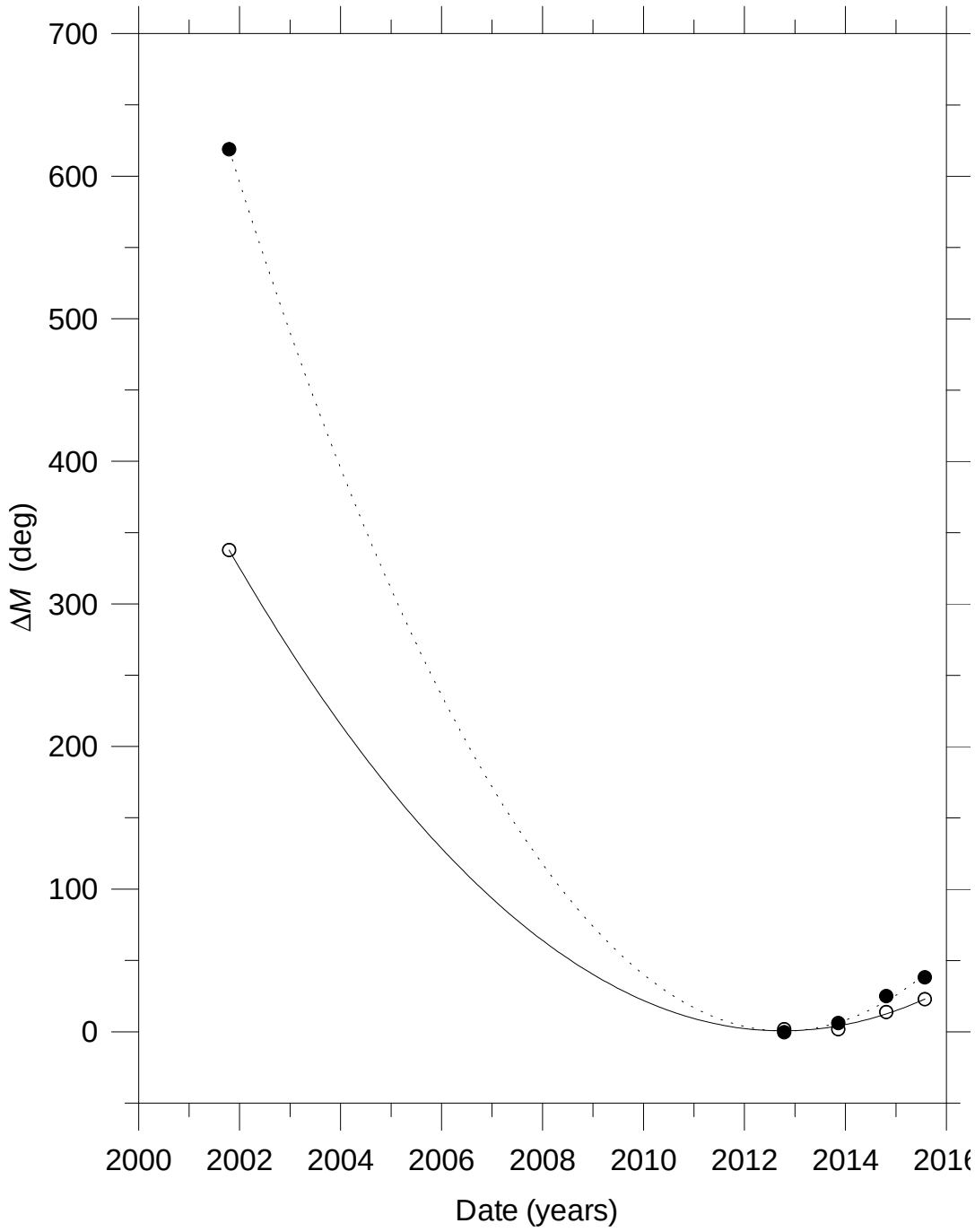

Fig. 8. Time evolutions of the mean anomaly difference ΔM between the best-fit solution with a constant orbital period (i.e., with ΔM_d fixed at zero) and the two best-fit solutions with ΔM_d fitted for (88710) 2001 SL9. Each point corresponds to the middle of one of the five apparitions from 2001 to 2015. The open and solid circles stand for the two solutions with $\Delta M_d = 2.8$ and 5.2 deg/yr^2, respectively. The sizes of the symbols in vertical direction represent estimated 3σ uncertainties in the timing of events ($\pm 5^\circ$ in mean anomaly). The solid line is a quadratic fit to the data points.

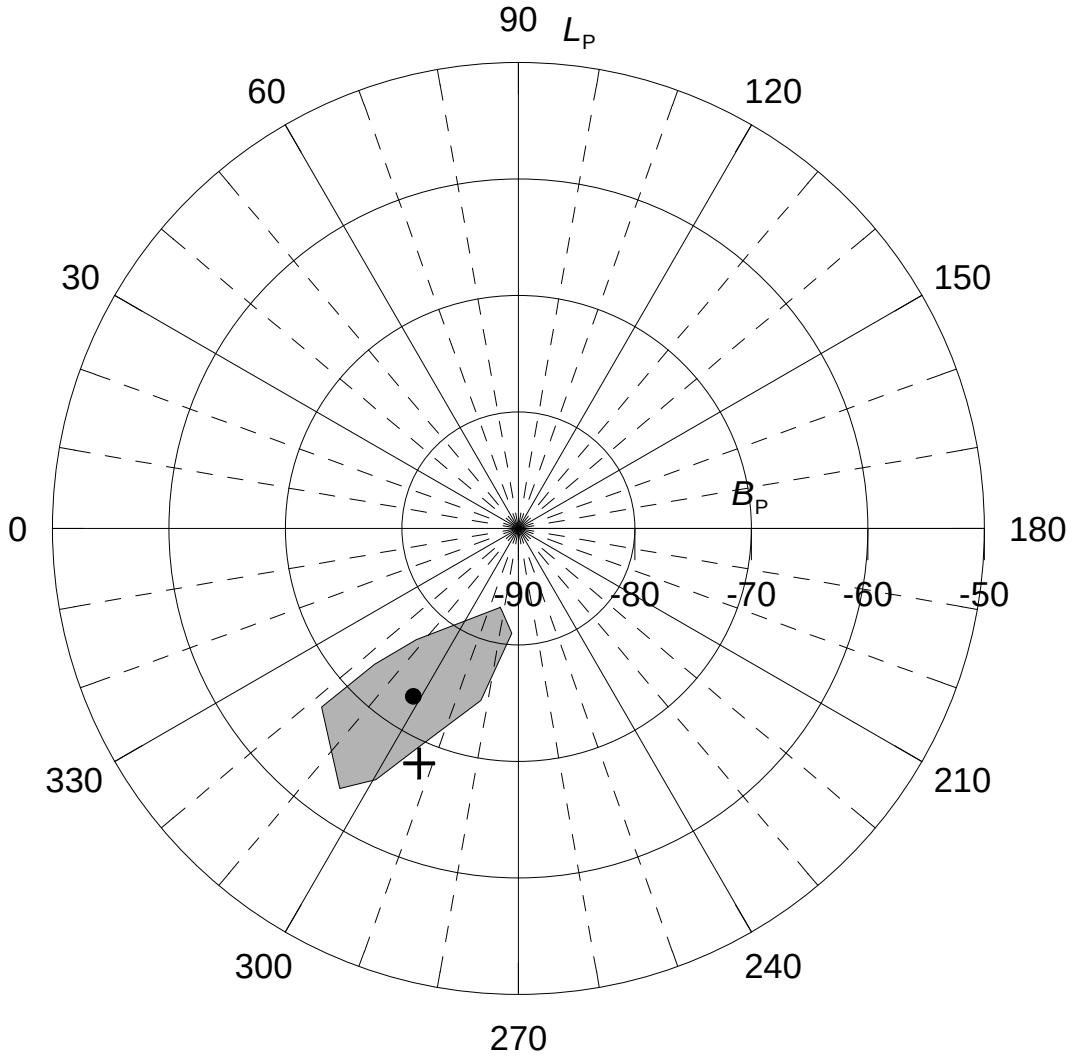

Fig. 9. Area of admissible poles for the mutual orbit of (88710) 2001 SL9 in ecliptic coordinates (grey area). The dot is the nominal solution given in Table 5. This area corresponds to 3σ confidence level. The south pole of the current asteroid's heliocentric orbit is marked with the cross.

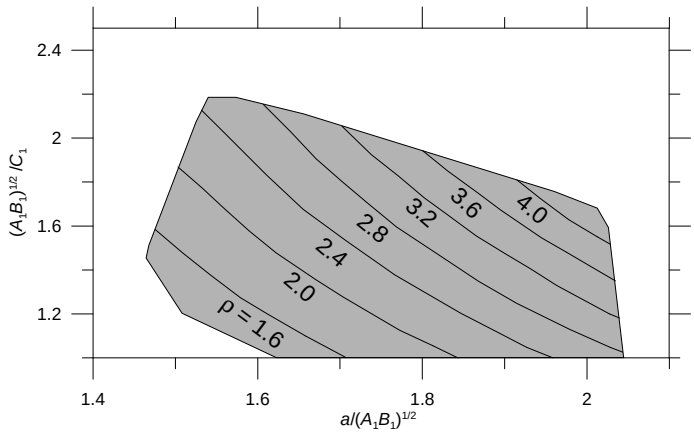

Fig. 10. Area of admissible combinations of the ratio between the mean equatorial and the polar axes of the primary ($(A_1B_1)^{1/2}/C_1$) and the semimajor axis of the mutual orbit a of (88710) 2001 SL9. This area corresponds to 3σ confidence level. Values of the bulk density of the system (ρ) in g cm^{-3} are indicated.